

## Full paper

# Cowpea-structured PVDF/ZnO nanofibers based flexible self-powered piezoelectric bending motion sensor towards remote control of gestures



Weili Deng<sup>1</sup>, Tao Yang<sup>1</sup>, Long Jin, Cheng Yan, Haichao Huang, Xiang Chu, Zixing Wang, Da Xiong, Guo Tian, Yuyu Gao, Haitao Zhang, Weiqing Yang\*

Key Laboratory of Advanced Technologies of Materials (Ministry of Education), School of Materials Science and Engineering, State Key Laboratory of Traction Power, Southwest Jiaotong University, Chengdu 610031, PR China

## ARTICLE INFO

## Keywords:

PVDF/ZnO  
Cowpea-structured nanofiber  
Bending monitoring  
Self-powered  
Human-machine interaction

## ABSTRACT

Interactive human-machine interface (iHMI) is a bridge connecting human beings and robots, which has an important requirement for perceiving the change of pressure and bending angle. Here, we designed a flexible self-powered piezoelectric sensor (PES) based on the cowpea-structured PVDF/ZnO nanofibers (CPZNs) for remote control of gestures in human-machine interactive system. Due to the synergistic piezoelectric effect of hybrid PVDF/ZnO and the flexibility of polymer, this PES exhibited excellent bending sensitivity of  $4.4 \text{ mV deg}^{-1}$  ranging widely from  $44^\circ$  to  $122^\circ$ , fast response time of 76 ms, and good mechanical stability. Besides, the PES could operate under both bending and pressing mode, show ultrahigh pressing sensitivity of  $0.33 \text{ V kPa}^{-1}$ , with response time of 16 ms. When integrated in iHMI, the PES could be conformably covered on different curve surfaces, demonstrated accurate bending angle recording and fast recognition for realizing intelligent human-machine interaction. On this basis, the application of remote control of robotic hand was successfully realized in form of acting the same gesture as human hand synchronously. This CPZNs-based self-powered PES is distinct and unique in its structure and fundamental mechanism, and exhibits a prospective potential application in iHMI.

## 1. Introduction

An interactive human-machine interface (iHMI) enables humans to control hardware and collect feedback information, which is a bridge between human and machine, have attracted extensive attentions and developed rapidly in recent years [1–10]. Generally, iHMI is a bidirectional electronic system that connects human and machines, allowing for the effective transfer of human intentions to the machine and the collection of feedback information from the machine [11,12]. In iHMI, flexible pressure and bending angle sensors are considered as the most important components in the applications like soft robotics [13] and gesture recognition [14]. Currently, pressure sensors are developing quickly, but there are few reports about bending angle sensors, especially, those can be used for quantitative measurement with wide range. Furthermore, when these sensors are integrate into the iHMI to mimic the comprehensive properties of human skin, they need to be conformably covered on the human body, and even be integrated with skin-like battery or self-sustainable power source [15–22].

Presently, the pressure and bending angle sensors are mostly based

on the mechanism of force-induced change in one typical parameter, for example resistance [23], capacitance [24], piezoelectric output [25,26], or triboelectric output [27–29]. Around different working principles, different materials such as metal nanowires [30–32], carbon nanotubes- or graphene-based materials [33–35], and conducting polymers [36] have been proposed for pressure and bending angle measurement. Although these sensors could detect the actions produced by human activities, voltage supply to operate these sensors is inevitable [37], which is one critical obstacle for wearable sensors in iHMI [38]. Among them, piezoelectric sensor that can directly generate electrical signals in response to mechanical force, facilitating the realization of a self-powered sensor system, has been considered as one of the most promising candidates to solve the power consumption issue of wearable electronic devices. However, traditional piezoelectric PZT [39] and AlN [40] based pressure sensors are not compatible with flexible substrates due to the high fabrication temperature and inherent brittleness, which can hardly achieve bending measurement. Although new fabrication process [25] was adopted to fabricate the flexible sensors based on the inorganic piezoelectric ceramic, the ability to

\* Corresponding author.

E-mail address: [wqyang@swjtu.edu.cn](mailto:wqyang@swjtu.edu.cn) (W. Yang).

<sup>1</sup> Weili Deng and Tao Yang contributed equally to this work.

measure bending angle is still limited to its intrinsic instability. Besides, polymer-based [41] piezoelectric sensors, such as poly (vinylidene fluoride) (PVDF), have also been reported with good flexibility, but they exhibit low sensitivity because of intrinsically poor piezoelectric properties. In addition, current reports on the detection of bending are mostly qualitative measurements [42–45], just judging whether there is

a bending or not, but less quantitative detection of bending angles [46]. Hence, to realize quantitative measurement of bending angle with self-powered ability in iHMI is still a big challenge.

In this study, we presented a flexible self-powered piezoelectric sensor (PES) for the quantitative measurement of bending angle based on CPZNS with the unique cowpea structure via electrospinning

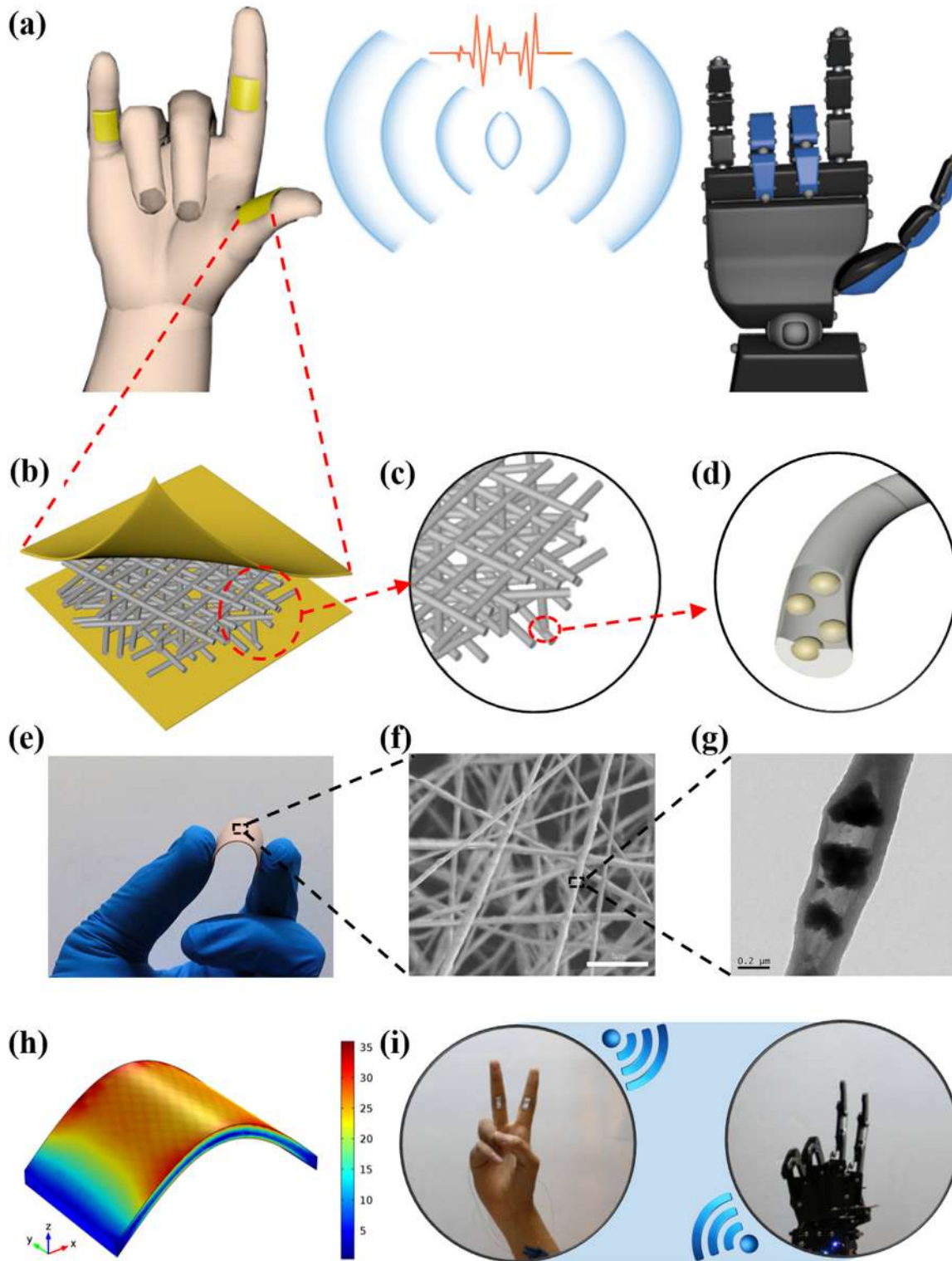


**Fig. 1.** The structure design of the CPZNS-based self-powered PES. (a) The schematic diagram of the developed smart sensor applied in the field of iHMI. The sketch of the device (b), NFs film (c) and a single NF (d). (e) The photograph of the fabricated sensor under bending mode. (f) The SEM image of the NFs. (g) The TEM image of a single NF. (h) The result of the FEM simulation. (i) The application of robot hand remote control based on the PES.

technology, and successfully demonstrated the application of PES for remote control of gesture in iHMI. The performance of PES was systematically studied both theoretically and experimentally. As a result, the designed PES could operate under both bending and pressing modes, and the sensitivity of PES could be easily regulated through the ratio of ZnO to PVDF. The optimum bending sensitivity of  $4.4 \text{ mV deg}^{-1}$  with a fast response time of 76 ms can be achieved ranging from  $44^\circ$  to  $122^\circ$ . On this basis, the fabricated flexible PES was respectively attached on the spring-grip and book to detect the power of gripping and the bending angle under the stage of opening or closing a book.

Moreover, when the PES integrated with signal processing circuit, the real-time wireless control of the robot hand was successfully realized. This work brings a novel cowpea-structured PVDF/ZnO nanofibers-based self-powered PES to the application field of interactive human-machine interface, and it will be believed to be an excellently prospective application for meeting the future challenges of iHMI.

## 2. Results and discussion

The structure design of the CPZNS-based self-powered piezoelectric

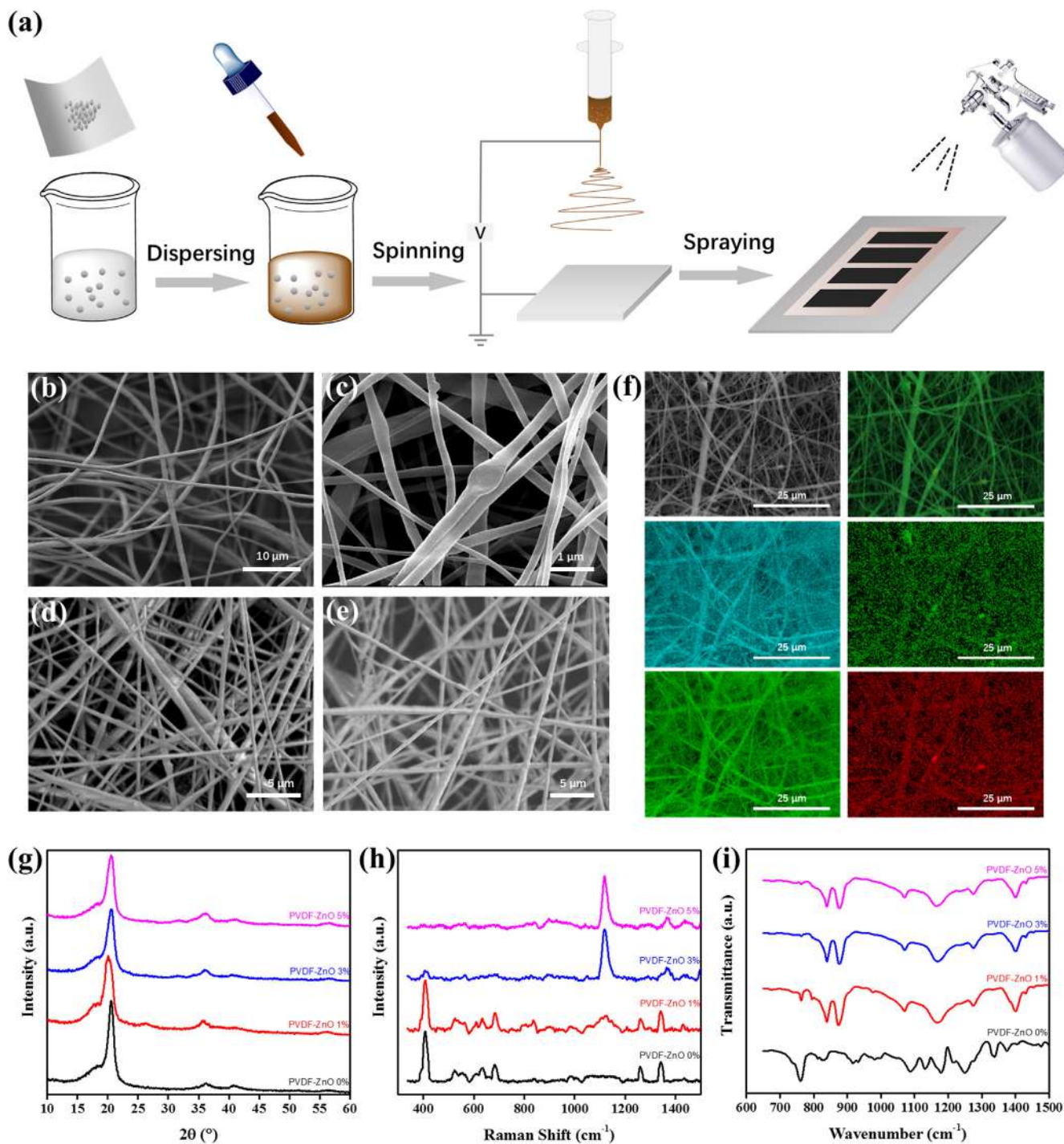


**Fig. 2.** Illustration characterizing the CPZNS of PES. (a) The fabrication process of PVDF/ZnO flexible sensor. The SEM image of PVDF/ZnO with ZnO content of 0 wt % (b), 1 wt% (c), 3 wt% (d), PVDF/ZnO 5wt% (e). (f) The EDS images of PVDF/ZnO NFs. (g) The XRD patterns of PVDF/ZnO NFs. (h) The Raman spectra of PVDF/ZnO NFs. (i) The FTIR spectra of PVDF/ZnO NFs.

sensor is shown in Fig. 1. As illustrated in Fig. 1a, the designed PES schematically realized the gesture remote control in human-machine interactive system. These as-fabricated PESs (Fig. 1b) are fixed on the inner side of human finger knuckles, and the robot fingers will be controlled to do the same bending action as human fingers based on the

relationship between the electrical output and the bending angle of the PES. To achieve this function, we innovatively designed a PVDF/ZnO nanofiber (NF) with the unique cowpea structure, and its detail structure design is schematically illustrated in Fig. 1d, where the ZnO nanospheres are well wrapped in PVDF NF like cowpea. And the results of

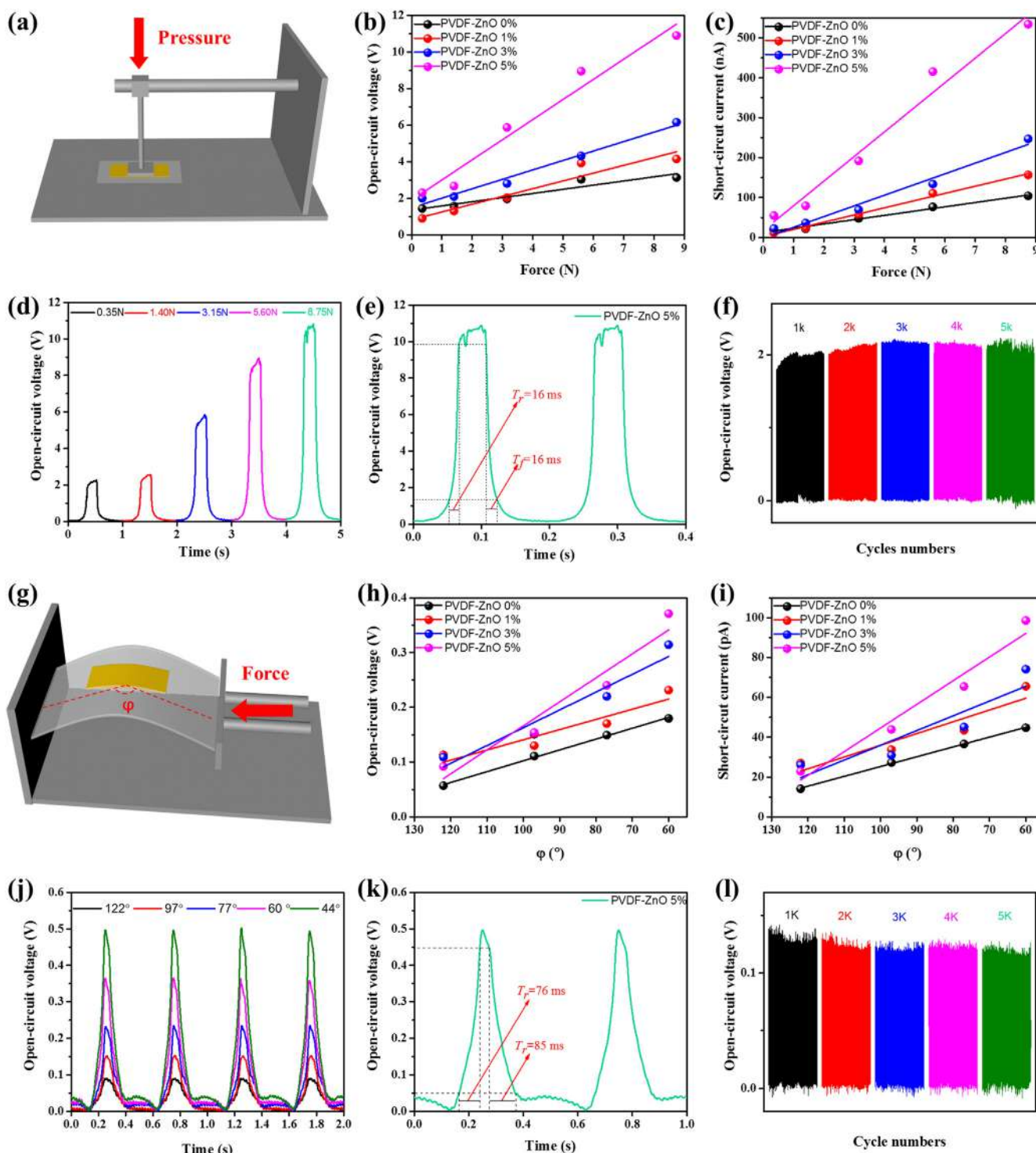


Fig. 3. Electrical characteristics of the designed PES. (a) The schematic diagram showing the measurement of PES under pressing model. Dependence of the open-circuit voltage (b) and short-circuit current (c) of PES with different force ranging from 0.35 N to 8.75 N. (d) The enlarge view of the open-circuit voltage under pressing in one period with different forces. (e) The rise/fall times of PES during the pressing model. (f) The mechanical durability test of PES under repeated pressing/unpressing conditions with force of 4.67 kPa for 5000 cycles. (g) The schematic diagram showing the measurement of PES under bending model. Dependence of the open-circuit voltage (h) and short-circuit current (i) of PES with different angle ( $\varphi$ ) ranging from 122° to 44°. (j) The enlarge view of the open-circuit voltage under bending in one period with different angles. (k) The rise/fall times of PES during the bending model. (l) The mechanical durability test of PES under repeated bending/unbending conditions with angles of 97° for 5000 cycles.

scanning electron microscope (SEM, Fig. 1f) and transmission electron microscopy (TEM, Fig. 1g) further confirmed the designed cowpea-structure of NFs. On this basis, the fabricated PVDF/ZnO NFs film (Fig. 1c) and flexible MXene ( $\text{Ti}_3\text{C}_2$ ) electrode were constructed the sandwich-like PES as demonstrated in Fig. 1b. Due to the flexibility of polymer and electrode, the fabricated PES exhibited good mechanical flexibility as shown in Fig. 1e. To further investigate the performance of this unique piezoelectric material, a bending-induced piezoelectric model was constructed to theoretically analyze the electrical output and the stress distribution through finite element method (FEM). As shown in Fig. 1h and Fig. S1 (Supporting information), it is easy to find that when device is bending under the external force, the stress is mainly concentrated at the bending position of the device and the voltage potential is generated on the opposite sides of the device. Therefore, the bending sensing can be theoretically realized based on the piezoelectric effect. Taking advantage of this performance, the self-powered PESs were stuck on human fingers to remotely and real-time control the robot hand to do the same gesture as human fingers. As illustrated in Fig. 1i, when the human hand give a gesture of ‘Two’, the robot hand will then complete the same action.

In order to prepare high-performance nanofibers, a facile and efficient electrospinning technique was selected to produce CPZNs. Fig. 2a illustrates the fabrication process of the flexible self-powered piezoelectric sensor based on the CPZNs. First, a certain proportion of ZnO and PVDF are dispersed in the mixture of acetone and dimethylacetamide (DMAC), and then the obtained mixture are used as precursors for electrospinning. Afterwards, the water solution of  $\text{Ti}_3\text{C}_2$  is sprayed on both sides of the spun film to be served as electrodes (The detail was shown in Experimental section). Notedly, the films prepared by electrospinning are usually porous, if the electrode is prepared by conventional evaporation or magnetron sputtering, the breakover between the upper and lower electrodes can easily occur in such sandwich structure. While many MXene and MXene-based composite films have been reported as electrodes for energy storage devices, and its conductivity is almost not affected by mechanical deformations, even bending or twisting [47]. In this regard, combining the unique hydrophobicity of PVDF [48], we spray the MXene water solution on the surface of the spun film as a stress-match electrode, which effectively overcomes the short circuit problem of traditional electrode. Finally, after extracting the electrode by copper wire, the device is completed.

The surface morphology of the electrospun PVDF/ZnO piezoelectric NFs is examined using scanning electron microscopy and energy dispersive spectroscopy (EDS). The continuous fiber sheets with ZnO content of 0%, 1%, 3% and 5% (weight ratio) were successfully obtained, as shown in Fig. 2b–e, respectively. From the SEM images, it can be seen that all the proportions of the mixed solution can be electrospun into a film and all the ZnO nanospheres (SEM image was shown in Fig. S2) are distributed uniformly in the PVDF matrix with no agglomeration. Furthermore, this conclusion is further confirmed by the TEM image (Fig. 1g) and EDS image (Fig. 2f). From Fig. 1g, it is explicit that the ZnO nanoparticles are well wrapped in PVDF NF, which is very similar to cowpea in structure. Especially, EDS image (Fig. 2f) reveals clearly that the zinc and oxygen elements are well distributed in the PVDF matrix. And the as-spun NF of 5 wt% provided a fiber diameter about  $0.5\ \mu\text{m}$ , which is originated from the statistical results of Fig. S3 (Supporting information).

The structural properties of the as-spun hybrid PVDF/ZnO fibers and its components were characterized by X-ray diffraction technique (XRD) and the obtained patterns are shown in Fig. 2g and Fig. S4 (Supporting information). From Fig. S4, it can be seen that all the diffraction peaks are well matched with the joint committee on powder diffraction standard (JCPDS: 99-0111) which indicates the wurzite structure of the ZnO. Compared with Fig. 2g, it is easy to find that the relative intensity of the diffraction peak of  $36.2^\circ$  (indicative of ZnO) increases with the increase of ZnO concentration. The peak at  $20.6^\circ$  ( $200/110$ ) corresponds to the  $\beta$ -crystalline phase of PVDF, which is

consistent with the literature report [49]. However, it is not clear whether the increase of ZnO concentration enhanced the  $\beta$ -phase of PVDF/ZnO. Hence, the crystallinity of PVDF/ZnO NFs were further analyzed by Raman spectra and Fourier transform infrared (FTIR) spectra. As shown in Fig. 2h, the Raman spectra of hybrid PVDF/ZnO NFs exhibits an obviously enhanced peak located at  $1147\ \text{cm}^{-1}$  with the increase of ZnO concentration, which is one characteristic peak of ZnO. Compared with the pure PVDF NF, the relative intensities of the bands at  $839\ \text{cm}^{-1}$  (indicative of  $\beta$ -phase) has increased from 1 to 2.9 in the hybrid PVDF/ZnO NF when the content of ZnO is 5 wt%. The more detailed comparison is further explicated in Fig. S5 (Supporting information). Additionally, the FTIR spectra is represented in Fig. 2i. Their vibrational peaks are observed at  $1270, 840, 878\ \text{cm}^{-1}$ , corresponding to the  $\beta$ -phase crystalline structures [50]. It is also clear from the FTIR spectra that the peak intensities at  $1270, 840, 878\ \text{cm}^{-1}$  for the doped samples is correspondingly higher than those of neat PVDF NFs. These results are also in excellent agreement with the reported literature [51]. Furthermore, both the increase of ZnO concentration and the  $\beta$ -phased PVDF are conducive to the improvement of PVDF/ZnO NFs electrical performance. On one hand, the additional ZnO nanospheres will enhance the locally electrical field during the electrospinning process, which induces the greater amount of  $\beta$ -phase crystalline compared with the neat PVDF NF [52]. On the other hand, the synergistic piezoelectric effect of ZnO and PVDF will also promote the better electrical performance of the device. As expected, the higher the content of  $\beta$ -phased PVDF and ZnO concentration, the better the electrical output of PES. So, we chose different proportions of the electrospun hybrid PVDF/ZnO fiber mat to verify the performance of sensors during the subsequent experiments.

In order to further investigate the electrical output performance of the as-fabricated PES, an electromechanical platform was used to simulate external compressive forces under different working modes of pressing and bending, and the schematic diagram of the test system is shown in Figs. 3a and g, respectively. While the force loading is increasing on the as-fabricated sensors, the quantitative electrical output of the sensor could be acquired through a measuring meter and a data acquisition system. The detailed schematic diagram was shown in Fig. S6 (Supporting information). Specifically, in pressing mode, Fig. 3d plots representative open-circuit voltage response curves of the PES under different compressive forces with the frequency of 1 Hz. Here, it is obvious that the output voltage of the PES increased with the compressive force. Based on these results, the electrical output performances of PES with different component proportions as a function of loading forces were illustrated in Figs. 3b and 3c. From the results, both the open-circuit voltage and the short-circuit current show the same trend, that is, both the voltage and current increase with the increase of external force, even if the component proportion of the sensor are different. The voltage sensitivity of the device, ( $S = \Delta V/\Delta P$ , where  $\Delta P$  is the relative change of applied pressure, and  $\Delta V$  is the relative change of output voltage), can be obtained by the linear slope of the plot [53], and the highest sensitivity of  $0.33\ \text{V kPa}^{-1}$  can be achieved when the content of ZnO was 5 wt%, which is obviously superior to the other literature [54]. At ranges of pressing force between 0.35 and 8.75 N, corresponding pressure of 1–30 kPa, the devices show good sensitivity and linearity. And the open-circuit voltage and short-circuit current of the devices with different contents of ZnO were further detailed shown in Figs. S7 and S8 (Supporting information). While in bending mode, the electrical output performances of sensors as a function of bending angles were illustrated in Fig. 3j. It is clearly observed that the output voltage increases with the decrease of the bending angle. The further experimental results show that the open circuit voltage and short-circuit current have the same trend as pressing mode when the device is bending, as exhibited in Figs. 3h and 3i. Meanwhile, it can be seen that the higher the content of ZnO, the better the electrical performance of the device, when the bending angle ranging from  $122^\circ$  to  $44^\circ$ , with different bending radii of 22.65–9.16 mm. Analogous to pressing mode,

we can also define the sensitivity of bending mode, ( $S = \Delta V / \Delta \varphi$ , where  $\Delta \varphi$  is the relative change of bending angle, and  $\Delta V$  is the relative change in output voltage), which can be obtained by the linear slope of the plot. It is resulted that the highest sensitivity of  $4.4 \text{ mV deg}^{-1}$  can be achieved by the ZnO content of 5 wt% sample. Based on this relationship between the output voltage and bending angle, the PES could achieve quantitative measurement of bending angle. The further detail

about the open-circuit voltage and short-circuit current of the PESs with different contents of ZnO can be found in Figs. S9 and S10 (Supporting information). As expected, according to analysis of material properties, the higher the content of  $\beta$ -phased PVDF and ZnO concentration, the better the electrical output, which was verified by the results of the experiments under both pressing and bending modes. In addition, when the response time of the PES were defined as the rise time ( $T_r$ ) of the

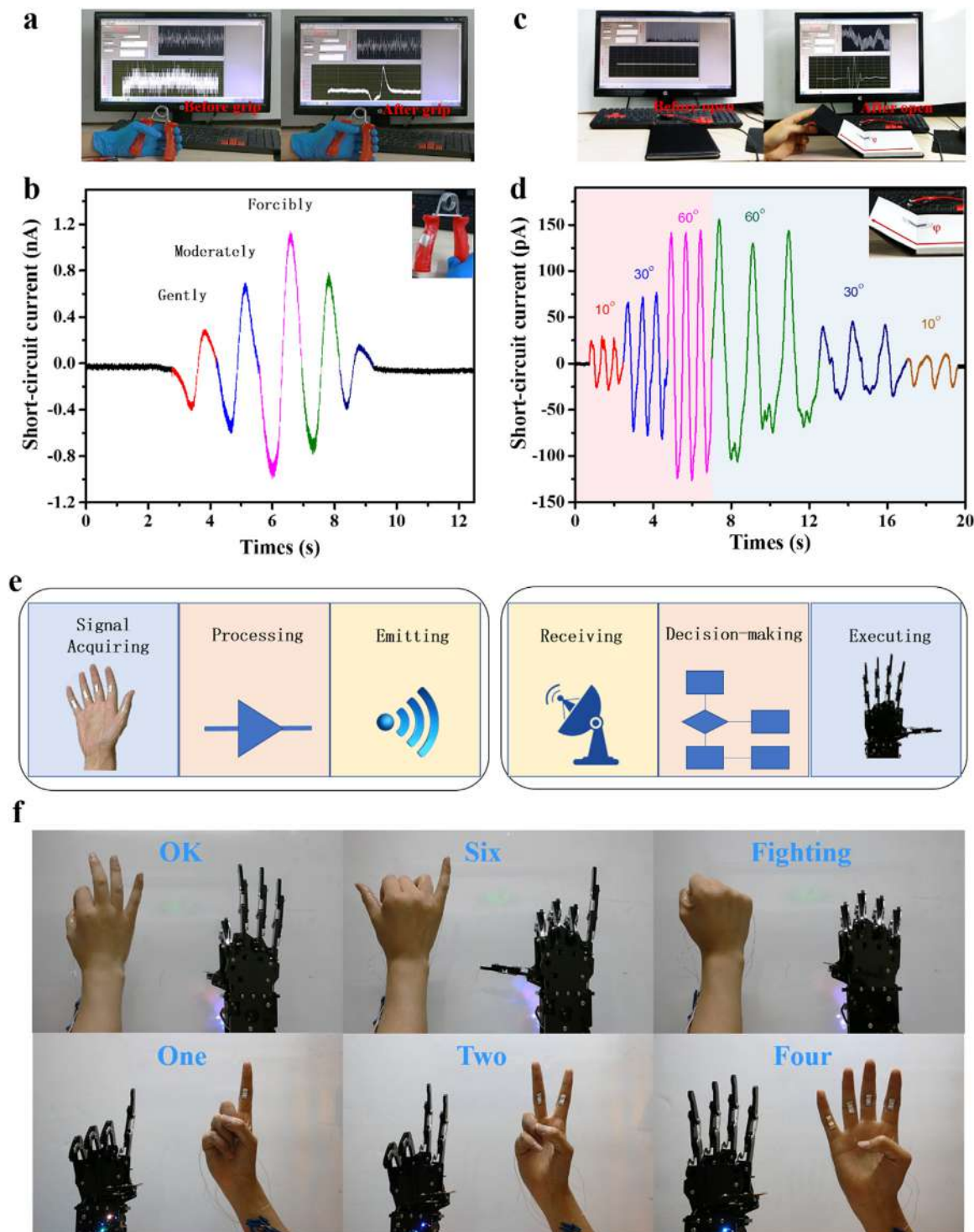


**Fig. 4.** The applications of the designed PES for iHMI. (a) Photograph of the PES conformably attached to the spring-grip to detect the power of gripping. (b) Short-circuit current output of PES under different grip strength. (c) Photograph of PES placed on the book to detect the angle of the opening/closing book. (d) Short-circuit current output of PES under the stage of closing (red area) and opening (blue area) a book. (e) Schematic diagram of a human-machine remote control system. Several simple electric modules were adopted to realize the gesture remote control. (f) The application of the gesture remote control based on PES.

voltage increasing from 10% to 90% or the fall time ( $T_f$ ) of the voltage decreasing from 90% to 10%, from the relationship of open-circuit voltage versus time, it can be observed that the  $T_r/T_f$  were about 16/16 ms (pressing mode, Fig. 3e) and 76/85 ms (bending mode, Fig. 3k), whose results are comparable to the recently reported self-powered sensors [25,53]. Moreover, the mechanical durability of the sensor was verified by a dynamic loading test for 5000 cycles under the pressure of 4.67 kPa at 2 Hz (Fig. 3f) and a bending test for 5000 cycles with bending angle of 97° at 2 Hz (Fig. 3l) respectively. Both the generated output voltages display no noticeable fluctuation during the repetitive loading tests, evidently revealing that the fabricated device has good mechanical and electrical stability, which are attributed to the good mechanical flexibility of PVDF and the synergistic piezoelectric effect of CPZNs.

The excellent electrical performance, mechanical stability and flexibility of the CPZNs make them good candidates to be integrated into various self-powered sensors in iHMI. In the following section, we further demonstrated potential uses of the presented CPZNs based self-powered piezoelectric sensors in various applications including real time grip strength measurement, bending angle monitoring, and human finger gestures remote control. Fig. 4a shows the photograph of the fabricated sensor used for real time grip strength measurement, and the PES was conformably attached on the spring-grip as shown in the inset of Fig. 4b. When a certain pressure was applied on PES, the corresponding electrical signal converted by the PVDF/ZnO NFs will be detected. From Fig. 4b, we can see that when the applied pressure increased/decreased, the output voltage of the PES changes accordingly with a very high sensitivity. The related video can be found in Movie S1 (Supporting information). Such an accurately strength measurement provides a great potential application value in tactile sensing [3]. Following, we further examined the as-fabricated PES as a bending motion sensing device, which is fixed on the folding line of a book as shown in Fig. 4c and the enlarge view of the application was shown in the inset of Fig. 4d. In detail, the electromechanical properties of PES were investigated by measuring the electrical output at different bending angle. The short-circuit current of PES was examined by opening the book at 10°, 30°, and 60° step by step and then closing gradually from 60° to 30° and 10° with different frequency. The relative change of short-circuit current was recorded in Fig. 4d. As can be seen, the PES could quantitatively distinguish the changes of bending angle and frequency with a quick response. The related video was shown in Movie S2 (Supporting information).

Supplementary material related to this article can be found online at doi:10.1016/j.nanoen.2018.10.049.

Due to the excellent performance of the bending response, the as-fabricated PES can monitor the motion of human fingers to realize the remote control of the robotic palm. As depicted in Fig. 4e, the fabricated sensors adhered to the inner side of finger knuckles can perceive the bending motion of human finger thus generate quantitative pulse signal, which is able to realize the wireless control of the robotic palm to do the same gesture as human fingers through the peripheral circuit modules including a signal processing module, an emitter, a receiver, a comparison circuit, and an executive module. To begin with, if there is a motion of human fingers, the original bending motion of human fingers will be converted to be quantitative analog signals by PES, and then the analog signals are acquired and processed including amplifying and filtering. These amplified signals are then fed into an analog-to-digital converter (ADC). The micro-controller would receive the digital signals from ADC module for further data processing and further pass the signals to the emitter. On the terminal of robotic hand, the receiver received the signals from the paired emitter and transmitted the signals to another micro-controller. If the amplitude of the received signals is higher than a specific threshold, the micro-controller will make decision and send a specified command to the executive module, which will control the robotic hand to do the same motion as human fingers. On basis of these circuits, it could realize gesture recognition

and remote control. The demonstration of the fabricated PES used for human-machine remote control are shown in Fig. 4f, which exhibited various gestures wireless synchronization between human fingers and robotic hands. As can be seen, the robotic hands accurately reflect the user's real hand posture such as different numbers (One, Two, Four, Six) or catchwords (OK, Fighting). The related video can be found in Movie S3 in Supporting information. Notably, both the pressing and bending test results indicated that this CPZNs based flexible self-powered sensor can provide a facile and efficient method for the quantitative monitoring of multiple stress/strain parameters in real-time, especially for elaborate human-machine interactive remote control.

Supplementary material related to this article can be found online at doi:10.1016/j.nanoen.2018.10.049.

### 3. Conclusion

In summary, we successfully fabricated the cowpea-structured PVDF/ZnO nanofibers through electrospinning and demonstrated its application of serving as a flexible self-powered piezoelectric sensor for pressure sensing and bending motion monitoring. The fabricated PES could work under both pressing and bending modes without external power supply, exhibited good flexibility and high sensitivity. The best pressing and bending sensitivity of the fabricated PES could achieve up to 0.33 V kPa<sup>-1</sup> with response time of 16 ms, and 4.4 mV deg<sup>-1</sup> with response time of 76 ms, respectively. Besides, the PES shows good mechanical stability within 5000 cycles under both working modes. Furthermore, the flexible PES could be conformably attached on the surface of spring-grip and the folding line of a book to demonstrate the ability of quantitatively detecting the grip strength and bending angle. More interestingly, a self-powered real-time gesture remote control system was further successfully implemented by wirelessly transmitting the pulse signal from human fingers to robotic palm based on PES. What's more, due to the excellent performance of PES, they can be easily integrated into measuring system, which offers great potential for physical signal monitoring, gesture sensing, and other applications in iHMI.

### 4. Experimental section

#### 4.1. Preparation of ZnO nanospheres

ZnO nanospheres are prepared by improving solution precipitation method [55]. The dimethylsulfoxide (DMSO) solution (30 ml) containing zinc acetate (3 mmol) was mixed with ethanol solution (10 ml) containing tetramethylammonium hydroxide (TMAH, 5.5 mmol), after stirring for 24 h, adding ethyl acetate (40 ml) and ethanolamine (160 μl), then separating the ZnO nanoparticles with the centrifuge (10,000 min<sup>-1</sup>) and dried in an oven at 60 °C.

#### 4.2. Preparation of hybrid PVDF/ZnO nanofibers

First, the appropriate amount of ZnO was added to the mixture of acetone and dimethylacetamide (DMAC), after ultrasonic dispersion for 2 h, the PVDF was added, and the obtained mixture was continued to be bathed for 6 h at 45 °C to be used as precursor solution of spinning. After the prepared solution poured into syringe, a 20 G metal needle was connected to the outlet of the syringe. And the syringe was mounted on a syringe pump, which provided a constant flowrate of 30 μl min<sup>-1</sup>. Electrospinning was performed at 17 kV, with a fixed distance of 15 cm between the tip of the spinneret and the collector. Then, the fabricated films were annealed for 2 h at 140 °C.

#### 4.3. Sensor fabrication

The powder of Ti<sub>3</sub>C<sub>2</sub> (0.2 g) is added to the deionized water (25 ml), and the precursor solution is obtained after ultrasonic dispersion for

1 h. Then, the obtained precursor solution is centrifuged for 1 h at  $3500 \text{ min}^{-1}$ , and the upper solution is sprayed on the both surfaces of as-spun film for 1 h with a designed mask under the spraying pressure of 0.1 MPa. After the copper wire is used to extract the electrode, the device is encapsulated by polyurethane (PU) film.

#### 4.4. Materials characteristics

Field emission scanning electron microscope (FESEM, JSM-7800F) and Transmission electron microscope (TEM, JEM-2100) were employed to observe the morphology of synthesized materials. The structural properties of the as-spun film were obtained from X-ray diffraction technique (XRD, X Pert Mpd pro). The Raman spectrum was obtained by utilizing confocal Raman spectroscopy (RM2000) at room temperature. The crystallinity of PVDF/ZnO NFs was further analyzed by Fourier transform infrared (FTIR, AVATAR360) spectra.

#### 4.5. Measurement of electric performance

The output voltage signals of PES were measured by a low-noise voltage preamplifier (Keithley-6514 system electrometer). The output current signals of PES were measured by a low-noise current preamplifier (Stanford Research SR570). And then the signals were collected and analyzed by the Data Acquisition Card (NI PCI-6221).

#### Acknowledgments

This work was financially supported by the National Natural Science Foundation of China (No. 61801403), the Scientific and Technological Projects for International Cooperation of Sichuan Province (No. 2017HH0069), the National Key Research and Development Plan (No. 2016YFB1200401-102E), the Independent Research Project of State Key Laboratory of Traction Power (No. 2017TPL\_Z04), and the Fundamental Research Funds for the Central Universities of China (Nos. 2682017CY06, 2682017ZDPY01 and 2682017CX071). Thanks for the help from the Analysis and Testing Center of Southwest Jiaotong University.

#### Supporting information

Supporting Information is available from the Elsevier Online Library or from the author.

#### Notes

The authors declare no competing financial interest.

#### Appendix A. Supporting information

Supplementary data associated with this article can be found in the online version at doi:10.1016/j.nanoen.2018.10.049.

#### References

- [1] S. Wang, J.Y. Oh, J. Xu, H. Tran, Z. Bao, *Acc. Chem. Res.* 51 (2018) 1033–1045.
- [2] H. Wu, Z. Su, M. Shi, L. Miao, Y. Song, H. Chen, M. Han, H. Zhang, *Adv. Funct. Mater.* 28 (2018) 1704641.
- [3] T. Yang, D. Xie, Z. Li, H. Zhu, *Mat. Sci. Eng. R* 115 (2017) 1–37.
- [4] A. Chortos, J. Liu, Z. Bao, *Nat. Mater.* 15 (2016) 937–950.
- [5] S. Lee, A. Reuveny, J. Reeder, S. Lee, H. Jin, Q. Liu, T. Yokota, T. Sekitani, T. Isoyama, Y. Abe, Z. Suo, T. Someya, *Nat. Nanotechnol.* 11 (2016) 472–478.
- [6] E. Roh, B.U. Hwang, D. Kim, B.Y. Kim, N.E. Lee, *ACS Nano* 9 (2015) 6252–6261.
- [7] S. Jung, J.H. Kim, J. Kim, S. Choi, J. Lee, I. Park, T. Hyeon, D.H. Kim, *Adv. Mater.* 26 (2014) 4825–4830.
- [8] J.W. Jeong, W.H. Yeo, A. Akhtar, J.J. Norton, Y.J. Kwack, S. Li, S.Y. Jung, Y. Su, W. Lee, J. Xia, H. Cheng, Y. Huang, W.S. Choi, T. Bretl, J.A. Rogers, *Adv. Mater.* 25 (2013) 6839–6846.
- [9] Y.-C. Lai, J. Deng, S.L. Zhang, S. Niu, H. Guo, Z.L. Wang, *Adv. Funct. Mater.* 27 (2017) 1604462.
- [10] K. Dong, J. Deng, W. Ding, A.C. Wang, P. Wang, C. Cheng, Y.-C. Wang, L. Jin, B. Gu, B. Sun, Z.L. Wang, *Adv. Energy Mater.* 8 (2018) 1801114.
- [11] S. Lim, D. Son, J. Kim, Y.B. Lee, J.-K. Song, S. Choi, D.J. Lee, J.H. Kim, M. Lee, T. Hyeon, D.-H. Kim, *Adv. Funct. Mater.* 25 (2015) 375–383.
- [12] H. Guo, X. Pu, J. Chen, Y. Meng, M.-H. Yeh, G. Liu, Q. Tang, B. Chen, D. Liu, S. Qi, C. Wu, C. Hu, J. Wang, Z.L. Wang, *Sci. Robot.* 3 (2018) 2516.
- [13] B. Mosaddegh, P. Polygerinos, C. Keplinger, S. Wennstedt, R.F. Shepherd, U. Gupta, J. Shim, K. Bertoldi, C.J. Walsh, G.M. Whitesides, *Adv. Funct. Mater.* 24 (2014) 2163–2170.
- [14] L. Dhakar, P. Pitchappa, F.E.H. Tay, C. Lee, *Nano Energy* 19 (2016) 532–540.
- [15] Z. Liu, D. Qi, G. Hu, H. Wang, Y. Jiang, G. Chen, Y. Luo, X.J. Loh, B. Liedberg, X. Chen, *Adv. Mater.* 30 (2018) 1704229.
- [16] Y. Jiang, Z. Liu, N. Matsuhisa, D. Qi, W.R. Leow, H. Yang, J. Yu, G. Chen, Y. Liu, C. Wan, Z. Liu, X. Chen, *Adv. Mater.* 30 (2018) 1706589.
- [17] G. Cheng, H. Zheng, F. Yang, L. Zhao, M. Zheng, J. Yang, H. Qin, Z. Du, Z.L. Wang, *Nano Energy* 44 (2018) 208–216.
- [18] J. Yang, F. Yang, L. Zhao, W. Shang, H. Qin, S. Wang, X. Jiang, G. Cheng, Z. Du, *Nano Energy* 46 (2018) 220–228.
- [19] W. Shang, G.Q. Gu, F. Yang, L. Zhao, G. Cheng, Z.L. Du, Z.L. Wang, *ACS Nano* 11 (2017) 8796–8803.
- [20] Z.-H. Lin, G. Cheng, Y. Yang, Y.S. Zhou, S. Lee, Z.L. Wang, *Adv. Funct. Mater.* 24 (2014) 2810–2816.
- [21] Y.F. Ai, Z. Lou, S. Chen, D. Chen, Z.M.M. Wang, K. Jiang, G.Z. Shen, *Nano Energy* 35 (2017) 121–127.
- [22] J.S. Lee, K.Y. Shin, O.J. Cheong, J.H. Kim, J. Jang, *Sci. Rep.* 5 (2015) 7887.
- [23] Y. Pang, K. Zhang, Z. Yang, S. Jiang, Z. Ju, Y. Li, X. Wang, D. Wang, M. Jian, Y. Zhang, R. Liang, H. Tian, Y. Yang, T.L. Ren, *ACS Nano* 12 (2018) 2346–2354.
- [24] T. Li, H. Luo, L. Qin, X. Wang, Z. Xiong, H. Ding, Y. Gu, Z. Liu, T. Zhang, *Small* 12 (2016) 5042–5048.
- [25] D.Y. Park, D.J. Joe, D.H. Kim, H. Park, J.H. Han, C.K. Jeong, H. Park, J.G. Park, B. Joung, K.J. Lee, *Adv. Mater.* 29 (2017) 1702308.
- [26] W. Deng, L. Jin, B. Zhang, Y. Chen, L. Mao, H. Zhang, W. Yang, *Nanoscale* 8 (2016) 16302–16306.
- [27] L. Jin, W. Deng, Y. Su, Z. Xu, H. Meng, B. Wang, H. Zhang, B. Zhang, L. Zhang, X. Xiao, M. Zhu, W. Yang, *Nano Energy* 38 (2017) 185–192.
- [28] B. Zhang, L. Zhang, W. Deng, L. Jin, F. Chun, H. Pan, B. Gu, H. Zhang, Z. Lv, W. Yang, Z.L. Wang, *ACS Nano* 11 (2017) 7440–7446.
- [29] W. Wang, J. Chen, X. Wen, Q. Jing, J. Yang, Y. Su, G. Zhu, W. Wu, Z.L. Wang, *A.C.S. Appl. Mater. Interfaces* 6 (2014) 7479–7484.
- [30] Y. Heo, Y. Hwang, H.S. Jung, S.H. Choa, H.C. Ko, *Small* 13 (2017) 1700070.
- [31] M. Amjadi, A. Pichitpajongkit, S. Lee, S. Ryu, I. Park, *ACS Nano* 8 (2014) 5154–5163.
- [32] S. Gong, W. Schwalb, Y. Wang, Y. Chen, Y. Tang, J. Si, B. Shirinzadeh, W. Cheng, *Nat. Commun.* 5 (2014) 3132.
- [33] L.Q. Tao, K.N. Zhang, H. Tian, Y. Liu, D.Y. Wang, Y.Q. Chen, Y. Yang, T.L. Ren, *ACS Nano* 11 (2017) 8790–8795.
- [34] X. Liao, Q. Liao, X. Yan, Q. Liang, H. Si, M. Li, H. Wu, S. Cao, Y. Zhang, *Adv. Funct. Mater.* 25 (2015) 2395–2401.
- [35] J. Park, Y. Lee, J. Hong, M. Ha, Y.D. Jung, H. Lim, S.Y. Kim, H. Ko, *ACS Nano* 8 (2014) 4689–4697.
- [36] Y. Cheng, R. Wang, K.H. Chan, X. Lu, J. Sun, G.W. Ho, *ACS Nano* 12 (2018).
- [37] G. Zhu, W.Q. Yang, T. Zhang, Q. Jing, J. Chen, Y.S. Zhou, P. Bai, Z.L. Wang, *Nano Lett.* 14 (2014) 3208–3213.
- [38] W. Gao, S. Emaminejad, H.Y.Y. Nyein, S. Challa, K. Chen, A. Peck, H.M. Fahad, H. Ota, H. Shiraki, D. Kiriya, D.H. Lien, G.A. Brooks, R.W. Davis, A. Javey, *Nature* 529 (2016) 509–514.
- [39] K.I. Park, J.H. Son, G.T. Hwang, C.K. Jeong, J. Ryu, M. Koo, I. Choi, S.H. Lee, M. Byun, Z.L. Wang, K.J. Lee, *Adv. Mater.* 26 (2014) 2514–2520.
- [40] M. Pătru, L. Isac, L. Cunha, P. Martins, S. Lanceros-Mendez, G. Oncioiu, D. Cristea, D. Munteanu, *Appl. Surf. Sci.* 354 (2015) 267–278.
- [41] Y.-K. Fuh, P.-C. Chen, Z.-M. Huang, H.-C. Ho, *Nano Energy* 11 (2015) 671–677.
- [42] M. Zhang, C. Wang, H. Wang, M. Jian, X. Hao, Y. Zhang, *Adv. Funct. Mater.* 27 (2017) 1604795.
- [43] H. He, Y. Fu, W. Zang, Q. Wang, L. Xing, Y. Zhang, X. Xue, *Nano Energy* 31 (2017) 37–48.
- [44] T.P. Huynh, H. Haick, *Adv. Mater.* 28 (2016) 138–143.
- [45] K.C. Pradel, W. Wu, Y. Ding, Z.L. Wang, *Nano Lett.* 14 (2014) 6897–6905.
- [46] Q. Shi, H. Wang, T. Wang, C. Lee, *Nano Energy* 30 (2016) 450–459.
- [47] S. Niu, Z. Wang, M. Yu, M. Yu, L. Xiu, S. Wang, X. Wu, J. Qiu, *ACS Nano* 12 (2018) 3928–3937.
- [48] W. Zhang, Z. Shi, F. Zhang, X. Liu, J. Jin, L. Jiang, *Adv. Mater.* 25 (2013) 2071–2076.
- [49] H. Parangusan, D. Ponnammam, M.A.A. Al-Maadeed, *Sci. Rep.* 8 (2018) 754.
- [50] M. Baniasadi, Z. Xu, S. Hong, M. Naraghi, M. Minary-Jolandan, *A.C.S. Appl. Mater. Interfaces* 8 (2016) 2540–2551.
- [51] S.K. Karan, R. Bera, S. Paria, A.K. Das, S. Maiti, A. Maitra, B.B. Khatua, *Adv. Energy Mater.* 6 (2016) 1601016.
- [52] D. Mandal, K. Henkel, D. Schmeisser, *Phys. Chem. Chem. Phys.* 16 (2014) 10403.
- [53] X. Wang, H. Zhang, L. Dong, X. Han, W. Du, J. Zhai, C. Pan, Z.L. Wang, *Adv. Mater.* 28 (2016) 2896–2903.
- [54] C. Pan, L. Dong, G. Zhu, S. Niu, R. Yu, Q. Yang, Y. Liu, Z.L. Wang, *Nat. Photonics* 7 (2013) 752–758.
- [55] X. Dai, Z. Zhang, Y. Jin, Y. Niu, H. Cao, X. Liang, L. Chen, J. Wang, X. Peng, *Nature* 515 (2014) 96–99.



**Weili Deng** received his M.E. degree from Chongqing University in 2009, and joined Southwest Jiaotong University as a teacher at the same year. In 2016, he received his Ph.D. in Materials Science and Engineering from Southwest Jiaotong University. His main research interest focuses on flexible electronics, such as pressure sensors and photoelectric detectors.



**Xiang Chu** received his B.E. degree in Materials Science and Engineering from Southwest Jiaotong University in 2016. He is now a doctoral candidate in Materials Science and Engineering at Southwest Jiaotong University. His research interest includes nano-materials for electrochemical energy storage devices.



**Tao Yang** received his B.E. degree in Materials Science and Engineering from Southwest Jiaotong University in 2017. He is currently pursuing master's degree in Materials Science and Engineering at Southwest Jiaotong University. His research focuses on the flexible electronics and self-powered sensors.



**Zixing Wang** received his B.E. degree in Materials Science and Engineering from Southwest Jiaotong University in 2017. He is now a master candidate in Materials Science and Engineering at Southwest Jiaotong University. His research interest includes nano-materials for electrochemical energy storage devices.



**Long Jin** received his B.E. degree from Southwest Jiaotong University in 2015. He is currently pursuing Ph.D. degree in Materials Science and Engineering at Southwest Jiaotong University.



**Da Xiong** received his B.E. degree in Materials Science and Engineering from Southwest Jiaotong University in 2018. Now he is a master candidate in Materials Science and Engineering at Southwest Jiaotong University. His recent research focuses on flexible optoelectronic devices and sensors.



**Cheng Yan** received his B.E. degree from Southwest Jiaotong University in 2017. He is currently pursuing Ph.D. degree in Materials Science and Engineering at Southwest Jiaotong University. His research focuses on the flexible electronics and self-powered sensors.



**Guo Tian** received his B.E. degree in Materials Science and Engineering from Southwest Jiaotong University in 2018. He is currently pursuing master's degree at Southwest Jiaotong University. His research interest includes piezoelectric materials and functional devices.



**Haichao Huang** received his B.E. degree in New Energy Materials and Devices from University of Electronic Science and Technology of China in 2016. He is a master candidate in Materials Science and Engineering at Southwest Jiaotong University in Weiqing Yang's group. His research interest includes all-solid-state electrochemical energy storage devices.



**Yuyu Gao** received his B.E. degree in Materials Science and Engineering from Southwest Jiaotong University in 2018. He is now a master candidate in Materials Science and Engineering at Southwest Jiaotong University. His research interest includes sensitive materials and functional devices.



**Haitao Zhang** received his Ph.D degree in Electrical Engineering from Institute of Electrical Engineering in 2015, Chinese Academy of Sciences. He is now an Assistant Prof. in Southwest Jiaotong University (Chengdu, China). His main research interest focus on new energy materials and their electrochemical energy storage devices including supercapacitors, Li-S batteries, and CO<sub>2</sub> batteries.



**Weiqing Yang** received his M.S. in Physics in 2007, and Ph.D. in Materials Science and Engineering from Sichuan University in 2011. He was a post-doctorate research fellow at University of Electronic Science and Technology of China from 2011 to 2013. Subsequently, he was a post-doctorate research fellow at Georgia Institute of Technology from 2013 to 2014, under the supervision of Prof. Zhong Lin Wang. His main research interest includes energy harvesting and storage devices, such as supercapacitors and nanogenerators.